*Particle Accelerators*, 1995, Vol. 49, pp. 221–251
Reprints available directly from the publisher
Photocopying permitted by license only



# ANALYTIC SOLUTION OF PARTICLE MOTION IN A DOUBLE RF SYSTEM*

J.Y. LIU, D.D. CAUSSYN, M. ELLISON, S.Y. LEE,
D. LI, A. RIABKO and L. WANG

*IUCF, Indiana University, Bloomington, IN 47405, USA*

*(Received 2 November 1994; in final form 18 January 1995)*

Analytic solutions for particle motion in a double rf system having a harmonic ratio of two are obtained. The effects of time dependent rf phase and voltage modulation on synchrotron motion are studied. Parametric resonances arising from a weak perturbation are analyzed in terms of the action-angle variables of the unperturbed Hamiltonian. Sum rules for the strength functions are derived. We find that the tree of bifurcation branches for these parametric resonances follows the characteristic tune of the unperturbed Hamiltonian. The basins of attraction for the dissipative double rf system are also studied in numerical simulations.

KEY WORDS: Double rf system, phase modulation, parametric resonance, bifurcation, sum rules, attractor

## 1 INTRODUCTION

Space charge has been an important limitation to beam intensity in many low energy proton synchrotrons. Space charge results in coherent and incoherent betatron tune shifts, which may lower the thresholds for transverse and longitudinal collective instabilities. A fast beam loss may occur during accumulation and storage when the injected beam current exceeds a threshold value. In many studies it was observed that the stability limit depended upon the rf voltage, momentum spread, vertical beam size, and nonlinear magnetic fields.[1]

To increase the threshold beam intensity, a double rf system has been used to increase the synchrotron frequency spread, which can enhance Landau damping against beam instabilities. An attempt to increase Landau damping was made as early as 1971 by installing a cavity operating at the third harmonic of the accelerating frequency in the Cambridge Electron Accelerator (CEA) at Cambridge.[2] This technique was successfully applied in the Intersecting Storage Rings (ISR) at the Center for European Nuclear Research (CERN) to cure coupled bunch mode instabilities, where an additional cavity was operated at the sixth harmonic of the primary rf frequency.[3]

*Work supported in part by the National Science Foundation contract NSF PHY-9221402 and the US Department of Energy contract DE-FG02-93ER40801.

Adding a higher harmonic rf voltage to the main rf voltage can flatten the potential well. Since the equilibrium beam profile follows the shape of potential well, a double rf system can provide a larger *bunching factor*,[4] defined as the fraction of the circumference occupied by a beam, than that of a single rf system. Therefore, for a given dc beam current in a synchrotron, the peak current and consequently the incoherent space charge tune shift are reduced. In particular, a double rf system with harmonics 5 and 10 was successfully used in the Proton Synchrotron Booster (PSB) at CERN to increase the beam intensity by 25–30% when the coherent longitudinal sextupole and decapole mode instabilities were suppressed by beam feedback systems.[5]

At Indiana University Cyclotron Facility (IUCF), a recent beam dynamics experiment showed that with optimized electron cooling the beam intensity in the cooler ring was quadrupled when two rf cavities were used.[6] This experiment has a far reaching consequences for low energy synchrotrons with electron cooling or stochastic cooling, where a high beam brightness may result in a severe space charge problem. Because a double rf system can improve beam intensity in synchrotrons, it is an important topic in accelerator physics.

With a double rf system, the synchrotron tune spread of a beam is increased for small amplitude oscillations. On the other hand, the synchrotron tune spread vanishes for particles having a phase amplitude $\phi$ of about 2 rad. The sextupole and decapole modes instabilities were observed and corrected by feedback systems in PSB.[5] This problem may arise from time-dependent rf phase and voltage modulation produced by rf noise, power supply ripple, synchro-betatron coupling, and wake fields. Since time-dependent perturbations can induce unstable longitudinal motion, careful studies are needed.

Previously, there have been some theoretical studies on double rf systems based on small amplitude approximations, which can not be extended to a large amplitude motion.[7,8] Clearly, we have to study large amplitude oscillations in order to understand the stability of particle motion. Recently, we have proposed a semi-analytic method to solve a double rf system beyond small amplitude approximations.[9] This paper makes further progress in understanding the beam dynamics for a double rf system analytically. When a double rf system is subject to an external perturbation, analytic solutions for the unperturbed Hamiltonian can provide a reliable basis for studying the effects of the perturbation on particle motion. Furthermore, sum rules for excitation spectrum due to the perturbation will be derived.

We organize this paper as follows. In Section 2, we present analytic solutions to the synchrotron motion in two rf systems. In Section 3, parametric resonances, driven by a rf phase modulation, are analyzed by expanding the perturbing potential in action-angle variables. With electron or stochastic cooling for phase space damping, these parametric resonances become attractors. Numerical simulations are used to study the basins of attraction. The parametric resonances due to a voltage modulation are discussed in Section 4. The conclusion is given in Section 5.

## 2 SYNCHROTRON MOTION

Without loss of generality, we consider the synchrotron equations of motion for particles below transition energy in a double rf system,

$$\dot{\phi} = \nu_s \delta, \tag{2.1}$$

$$\dot{\delta} = -\nu_s\{(\sin\phi - \sin\phi_{10}) - r[\sin(\phi_{20} + h(\phi - \phi_{10})) - \sin\phi_{20}] + v(\phi)_{sc}\} - \frac{\lambda}{2\pi}\delta, \tag{2.2}$$

where the dots are derivatives with respect to the orbiting angle $\theta$, $\phi$ is the phase coordinate relative to the primary rf cavity, $\delta = -\frac{h_1|\eta|}{\nu_s}\frac{\Delta p}{p}$ is the normalized momentum coordinate, $\frac{\Delta p}{p} = \frac{p-p_0}{p_0}$ is the fractional momentum deviation from the synchronous particle, $\eta$ is the phase slip factor, $\nu_s$ is the synchrotron tune at zero amplitude for the primary rf system alone given by $\nu_s = \sqrt{\frac{h_1 e V_1 |\eta|}{2\pi\beta^2 E_0}}$, $(h_1, h_2)$ and $(V_1, V_2)$ are respectively harmonic numbers and voltages of the primary and the secondary rf cavities with $h = \frac{h_2}{h_1}$ and $r = \frac{V_2}{V_1}$, and $\phi_{10}$ and $\phi_{20}$ are the corresponding rf phase angles of the synchronous particle. The effective acceleration rate for the beam is $\Delta E = eV_1(\sin\phi_{10} - r\sin h\phi_{20})$ per revolution. The term $eV_1 v(\phi)_{sc}$ denotes the energy shift due to space charge force per revolution, and $\frac{\lambda}{2\pi}\delta$ is the linearized phase space damping force due to electron or stochastic cooling with $\lambda$ as the damping coefficient. Because this study is devoted to single particle dynamics, we will ignore the space charge force.

Neglecting for the moment the damping effects, the Hamiltonian is given by

$$H = \frac{1}{2}\nu_s\delta^2 + V(\phi), \tag{2.3}$$

where the potential $V(\phi)$ is

$$V(\phi) = \nu_s\{(\cos\phi_{10} - \cos\phi) + (\phi_{10} - \phi)\sin\phi_{10} - \frac{r}{h}[\cos\phi_{20} - \cos(\phi_{20} + h(\phi - \phi_{10})) - h(\phi - \phi_{10})\sin\phi_{20}]\}. \tag{2.4}$$

Here, the conditions $r = \frac{1}{h}$ and $h\sin\phi_{20} = \sin\phi_{10}$ are needed to obtain a flattened potential well. For $r > \frac{1}{h}$, there are two inner buckets on the $\phi$ axis.

For the reason that the rf bucket is largest at the lowest harmonic ratio, this paper studies the double rf system with $h = 2$. To simplify our discussion, we study a stationary bucket with $\phi_{10} = \phi_{20} = 0°$. However, the method presented in this paper can be easily extended to the general case.

### *2.1 The action and the synchrotron tune*

When the synchrotron is operating at $\phi_{10} = \phi_{20} = 0$, the net acceleration is zero and the Hamiltonian becomes

$$H = \frac{\nu_s}{2}\delta^2 + \nu_s\left[(1 - \cos\phi) - \frac{r}{2}(1 - \cos 2\phi)\right]. \tag{2.5}$$

Since the Hamiltonian is autonomous, the "energy" $H = E$ of the Hamiltonian is a constant of motion with value $E/\nu_s \in [0, 2]$. The action is given by

$$J(E) = \frac{1}{\pi} \int_{-\hat{\phi}}^{\hat{\phi}} \delta d\phi, \tag{2.6}$$

where $\hat{\phi}$ is the maximum phase angle for a given Hamiltonian torus. The energy $E$ is related to $\hat{\phi}$ by $E = 2\nu_s(1 - 2r\cos^2\frac{\hat{\phi}}{2})\sin^2\frac{\hat{\phi}}{2}$, and the phase space area is $2\pi J$. The bucket area $\mathcal{A}_b$ is given by

$$\mathcal{A}_b = 2\pi\hat{J} = 8\left[\sqrt{1+2r} + \frac{1}{\sqrt{2r}}\ln(\sqrt{1+2r} + \sqrt{2r})\right], \tag{2.7}$$

which is a monotonic function of the ratio $r$. The corresponding bucket area for the single rf system is $\mathcal{A}_b(r \to 0) = 16$.

The synchrotron tune, defined as the number of synchrotron oscillations per revolution, is given by $Q_s = (\frac{\partial J}{\partial E})^{-1}$. Thus, we obtain

$$\frac{Q_s}{\nu_s} = \begin{cases} \dfrac{\pi\sqrt{(1-2r)+2t_0^2+(1+2r)t_0^4}}{2(1+t_0^2)K(k_1)}, & \text{when } r \le 0.5, \quad \text{or } r > 0.5, \text{ and } \hat{\phi} > \phi_b \\ \dfrac{\pi\sqrt{2r}t_u}{\sqrt{(1+t_u^2)(1+t_l^2)}K(k_2)}, & \text{when } r > 0.5, \ \hat{\phi} < \phi_b, \end{cases} \tag{2.8}$$

where $t_0 = \tan\frac{\hat{\phi}}{2}$, $t_u = \tan\frac{\phi_u}{2}$, $t_l = \tan\frac{\phi_l}{2}$, with $\phi_l = 2\arcsin\sqrt{\sin^2\frac{\phi_b}{2} - \sin^2\frac{\phi_u}{2}}$, $\phi_u = \hat{\phi}$, $\phi_b = 2\arccos(\frac{1}{\sqrt{2r}})$, $K(k)$ is the complete elliptical integral of the first kind. The moduli of the elliptical integral are $k_1 = \dfrac{t_0\sqrt{1+(1+2r)t_0^2}}{\sqrt{(1-2r)+2t_0^2+(1+2r)t_0^4}}$, and $k_2 = \dfrac{\sqrt{t_u^2-t_l^2}}{t_u}$. When $r > 0.5$, there are two stable fixed points located at $\pm\phi_f$ where $\cos\phi_f = \frac{1}{2r}$. Here $\phi_b$ corresponds to the maximum phase angle of the inner separatrix, $\phi_l$ and $\phi_u$ are the intercepts of the torus inside the inner separatrix. The detailed derivation of Eq. (2.8) is given in Appendix A.

Figure 1 shows the synchrotron tune as a function of the amplitude of the synchrotron oscillation for various voltage ratios. At $r = 0$, the system reduces to a single primary rf cavity, where the synchrotron tune is $Q_s/\nu_s = 1$ at zero amplitude. As $r$ increases, the first derivative of the synchrotron tune becomes large near the origin. Since a large tune spread of the beam is an essential ingredient for Landau damping of coherent beam instabilities, an optimal rf voltage ratio is $r = 0.5$, where the synchrotron tune spread of the beam is maximized for a given bunch area. At $r = 0.5$, the synchrotron tune becomes

$$\frac{Q_s}{\nu_s} = \frac{\pi t_0}{\sqrt{2(1+t_0^2)}K(k)} = \frac{\pi(E/2\nu_s)^{1/4}}{\sqrt{2}K(k)} \tag{2.9}$$

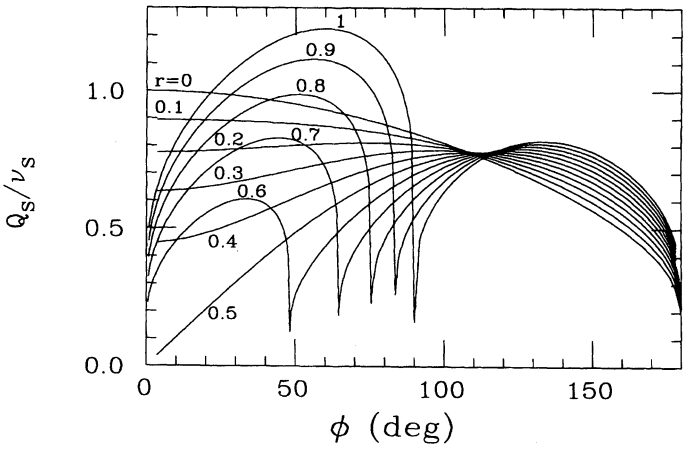


FIGURE 1: The synchrotron tune as a function of the peak phase $\phi=\hat{\phi}$ for different voltage ratio $r$.

with the modulus

$$k = \sqrt{\frac{1}{2}\left(1 + \frac{t_0^2}{1+t_0^2}\right)} = \sqrt{\frac{1}{2}\left(1 + \sqrt{\frac{E}{2\nu_s}}\right)}.$$

In this case, the maximum of the synchrotron tune is $\hat{Q}_s = 0.7786\nu_s$, located at $\hat{\phi} = 117°$ (or $E = 1.057\nu_s$). Near this region, $\frac{\partial Q_s}{\partial \hat{\phi}}$ is very small or zero. When the voltage ratio is $r > 0.5$, a dip in $Q_s(J)$ appears at the inner separatrix of inner buckets, and two small potential wells are formed inside the inner separatrix.

### 2.2 *Action-angle variables*

Although analytic solutions for action-angle variables, presented in this section, are valid only for the case with $r = 0.5$, the method can be extended to obtain similar solutions for other voltage ratios. Using the generating function

$$F_2(\phi, J) = \int_{\hat{\phi}}^{\phi} \delta(\phi')d\phi', \tag{2.10}$$

we obtain the angle variable as

$$\psi = \frac{\partial F_2}{\partial J} = \frac{\partial E}{\partial J}\int_{\hat{\phi}}^{\phi} \frac{\partial \delta}{\partial E}d\phi' = \frac{Q_s}{\nu_s}\int_{\hat{\phi}}^{\phi} \frac{d\phi'}{\delta}, \tag{2.11}$$

where the action variable is given in Eq. (2.6). Substituting $\delta$ into the integrand, the angle variable becomes (see Appendix B)

$$\psi = \frac{Q_s}{\nu_s}\frac{\sqrt{1+t_0^2}}{\sqrt{2}t_0}u = \frac{\pi u}{2K(k)}, \tag{2.12}$$

where the argument $u$ is related to the phase angle $\phi$ by

$$\tan\frac{\phi}{2} = \tan\frac{\hat{\phi}}{2}\mathrm{cn}u, \tag{2.13}$$

here $\mathrm{cn}u$ is a Jacobian elliptical function[10] with the modulus $k$

$$\mathrm{cn}u = \frac{2\pi}{kK(k)}\sum_{n=0}^{\infty}\frac{q^{n+1/2}}{1+q^{2n+1}}\cos(2n+1)\psi,$$

where $q = e^{-\pi K'/K}$, and $K' = K(k')$ with $k' = \sqrt{1-k^2}$.

The conjugate phase space variable $\delta$ can then be obtained from Hamilton's equation of motion, i.e.,

$$\delta = -2\sqrt{2}\sin\left(\frac{\hat{\phi}}{2}\right)\tan\left(\frac{\hat{\phi}}{2}\right)\frac{\mathrm{sn}u\ \mathrm{dn}u}{1+\left[\tan\frac{\hat{\phi}}{2}\mathrm{cn}u\right]^2}, \tag{2.14}$$

where $\mathrm{sn}u$ and $\mathrm{dn}u$ are Jacobian elliptical functions with modulus $k$. Thus the transformation of the phase space coordinates $(\phi, \delta)$ to the action-angle variables $(J, \psi)$ can be accomplished by using Eqs. (2.13) and (2.14) or equivalently the following equations,

$$\sin\frac{\phi}{2} = \frac{\xi^{1/4}\mathrm{cn}u}{\sqrt{1-\xi^{1/2}\mathrm{sn}^2u}}, \tag{2.15}$$

$$\frac{\delta}{2} = \pm\xi^{1/2}\sqrt{1-\frac{\mathrm{cn}^4u}{(1-\xi^{1/2}\mathrm{sn}^2u)^2}}, \tag{2.16}$$

where $\xi = \frac{E}{2\nu_s}$.

### 2.3 *Small amplitude approximation*

For a tightly bunched beam, the beam occupies a small phase space area. Formula for small amplitude approximation are summarized as follows:[7,9]

$$
\begin{aligned}
J &\approx \frac{8\sqrt{2}K}{3\pi}\left(\frac{E}{2\nu_s}\right)^{3/4} = \frac{8\sqrt{2}K}{3\pi}\sin^3\frac{\hat{\phi}}{2}, \\
\frac{Q_s}{\nu_s} &\approx \frac{\pi}{\sqrt{2}K}\sin\frac{\hat{\phi}}{2}, \\
\phi &\approx \hat{\phi}\frac{2\pi}{kK}\sum_{n=0}^{\infty}\frac{q^{n+1/2}}{1+q^{2n+1}}\cos(2n+1)\psi, \qquad (2.17) \\
\delta &= -\hat{\phi}^2\frac{\pi^2}{\sqrt{2}kK^2}\sum_{n=0}^{\infty}\frac{(2n+1)q^{n+1/2}}{1+q^{2n+1}}\sin(2n+1)\psi,
\end{aligned}
$$

where $k \approx \frac{1}{\sqrt{2}}$, $K = K(k) \approx 1.8541$ and $q \approx e^{-\pi}$.

Let the rms phase space area of the bunch be $\mathcal{A}$ and the rms conjugate phase space coordinates be $\sigma_\delta$ and $\sigma_\phi$. We obtain

$$
\sigma_\phi = \left(\frac{3\mathcal{A}}{2\sqrt{2}K}\right)^{1/3}, \quad \sigma_\delta = \left(\frac{3\mathcal{A}}{8K}\right)^{2/3}. \qquad (2.18)
$$

The rms tune spread of the beam is then given by

$$
\Delta Q = \frac{\pi}{\sqrt{2}K}\left(\frac{3\mathcal{A}}{16\sqrt{2}K}\right)^{1/3}\nu_s. \qquad (2.19)
$$

The approximate formula can be used to describe small amplitude oscillations. However it is more a concern when the beam fills the rf bucket, particles may become unstable at large synchrotron amplitudes. For the double rf system, subject to an external phase or voltage modulation, the motion may even become chaotic. Naturally one wants to know how particles behave when they have amplitude such that $\frac{Q_s}{\nu_s}$ is maximum and near the rf bucket boundary.

## 3 PHASE MODULATION

To study the stability of a Hamiltonian system, we apply a small time dependent perturbation. In this section, we study the effects of rf phase modulation, which may arise from rf noises, synchro-betatron coupling from the transverse dipole field modulation, and wake fields resulted from longitudinal impedances. With a sinusoidal phase modulation to the double rf system, Hamilton's equations of motion are given by

$$
\begin{aligned}
\dot{\phi} &= \nu_s\delta + a\nu_m\cos\nu_m\theta, \\
\dot{\delta} &= -\nu_s(\sin\phi - r\sin 2\phi),
\end{aligned} \qquad (3.1)
$$

where $\nu_m$ and $a$ are the modulation tune and amplitude respectively. The corresponding Hamiltonian is given by,

$$H = \frac{1}{2}\nu_s\delta^2 + \nu_s\left[(1-\cos\phi) - \frac{r}{2}(1-\cos 2\phi)\right] + a\nu_m\delta\cos\nu_m\theta. \tag{3.2}$$

When the perturbation is small with $a \ll 1$, the time dependent Hamiltonian can be expanded in action-angle variables of the unperturbed Hamiltonian.[9]

### *3.1 Analysis of parametric resonances*

To express the perturbation in terms of action-angle variables, we expand $\delta$ in Fourier series, i.e.,

$$\delta = \sum_{n=-\infty}^{\infty} g_n(J)e^{in\psi}, \tag{3.3}$$

where the *strength function* $g_n(J)$ is given by the inverse Fourier transform,

$$g_n(J) = \frac{1}{2\pi}\int_{-\pi}^{\pi}\delta e^{-in\psi}d\psi. \tag{3.4}$$

Since $\delta$ is a real and odd function of $\psi$, the phase modulation only gives rise to odd harmonic resonances from the first order perturbation with $g_{-n} = g_n^*$. The analytic expression for $g_n$ will be given in next section. Here we examine the effects of the perturbation on particle motion.

In terms of action-angle variables $(J, \psi)$, the Hamiltonian of Eq. (3.2) becomes

$$H = E(J) + a\nu_m\sum_{n\geq 0}|g_n(J)|\left[\cos(n\psi - \nu_m\theta + \chi_n) + \cos(n\psi + \nu_m\theta + \chi_n)\right], \tag{3.5}$$

where $E(J)$ is the energy of the unperturbed Hamiltonian, $a\nu_m|g_n|$ is the resonance strength of the $n$th order parametric resonance, and $\chi_n$ is the phase of $g_n$. When the modulation tune is near one of the parametric resonances, i.e., $\nu_m \approx n\dot{\psi}$, the resonance term contributes coherently to perturb particle motion. In order to see the perturbed Hamiltonian flow, we transform the Hamiltonian to the resonance rotating frame by using the generating function

$$W_2(\psi, I) = \left(\psi - \frac{\nu_m}{n}\theta + \frac{\chi_n}{n}\right)I, \tag{3.6}$$

where the new action angle variables become

$$I = J, \quad \text{and} \quad \gamma = \psi - \frac{\nu_m}{n}\theta + \frac{\chi_n}{n}. \tag{3.7}$$

The new Hamiltonian in the resonance rotating frame is given by $\mathcal{H} = \langle\mathcal{H}\rangle + \Delta\mathcal{H}$, where the time averaged Hamiltonian is

$$\langle\mathcal{H}\rangle = E(I) - \frac{\nu_m}{n}I + a\nu_m|g_n(I)|\cos n\gamma, \tag{3.8}$$

and the time dependent Hamiltonian is

$$\Delta\mathcal{H} = a\nu_m|g_n|\cos(n\gamma + 2\nu_m\theta) + a\nu_m \sum_{\ell\neq n,\ell\geq 1} |g_\ell| \left\{\cos\left[\ell\gamma + \left(\frac{\ell}{n} - 1\right)\nu_m\theta + \chi_\ell - \frac{\ell}{n}\chi_n\right] + \cos\left[\ell\gamma + \left(\frac{\ell}{n} + 1\right)\nu_m\theta + \chi_\ell - \frac{\ell}{n}\chi_n\right]\right\}. \tag{3.9}$$

Since the time dependent component contributes incoherently to particle motion, it can be averaged to zero. Therefore, we neglect it here for the moment.

Since the time averaged Hamiltonian $\langle\mathcal{H}\rangle$ is independent of $\theta$, it is a constant of motion. The structure of resonance islands can be described by the stable and unstable fixed points (SFP and UFP) given by the solutions of Hamilton's equations of motion, $\dot{I} = \frac{\partial\langle\mathcal{H}\rangle}{\partial\gamma} = 0$ and $\dot{\gamma} = -\frac{\partial\langle\mathcal{H}\rangle}{\partial I} = 0$. One obtains

$$\begin{aligned} n\gamma_{\mathrm{FP}} &= l\pi, \quad (l = 0, 1, 2, \ldots), \\ Q_s(I_{\mathrm{FP}}) - \frac{\nu_m}{n} &\pm a\nu_m|g_n'(I_{\mathrm{FP}})| = 0, \end{aligned} \tag{3.10}$$

where $(\gamma_{\mathrm{FP}}, I_{\mathrm{FP}})$ are phase space coordinates of fixed points and $g_n'$ is the derivative of the strength function. Since there are $n$ SFPs and $n$ UFPs, the number of resonance islands is equal to the order of resonance. The parametric resonances, given by Eq. (3.10), are therefore designated as the $n$:1 primary parametric resonances. For $a \ll 1$, the resonance condition becomes $\nu_m \approx nQ_s$.

The size of the resonance island is approximately given by

$$\Delta I \approx 4\left[\frac{\nu_m a|g_n(I)|}{|\frac{\partial Q_s}{\partial I}|}\right]^{1/2}_{I=I_r}, \tag{3.11}$$

where $I_r$ is the resonance action, i.e., $I_r = I_{\mathrm{SFP}}$. Thus, when $\frac{\partial Q_s}{\partial I} = 0$, the island size becomes large, and particle loss may occur.

### *3.2 Resonance strength function*

Using Eq. (2.13) and the coordinate transformation $d\psi = \frac{Q_s}{\nu_s\delta}d\phi$, the strength function $g_{2l+1}$ becomes (see Appendix C)

$$g_{2l+1} = i\frac{4Q_s}{\nu_s}\frac{(-)^l q^{l+1/2}}{1+q^{2l+1}}\cos\left[(2l+1)\frac{\pi u_0}{2K(k)}\right], \tag{3.12}$$

where $l = 0, 1, 2, \cdots$, and $u_0 = F(w, k)$ is the incomplete elliptical integral of the first kind with the upperbound of the integral given by $w = \arccos\left(\frac{k'}{k}\tan\frac{\hat{\phi}}{2}\right)$ and the modulus given by $k = \sqrt{\frac{1}{2}(1+\sin^2\frac{\hat{\phi}}{2})}$. Figure 2 shows the exact solution of $|g_n|$ with harmonics

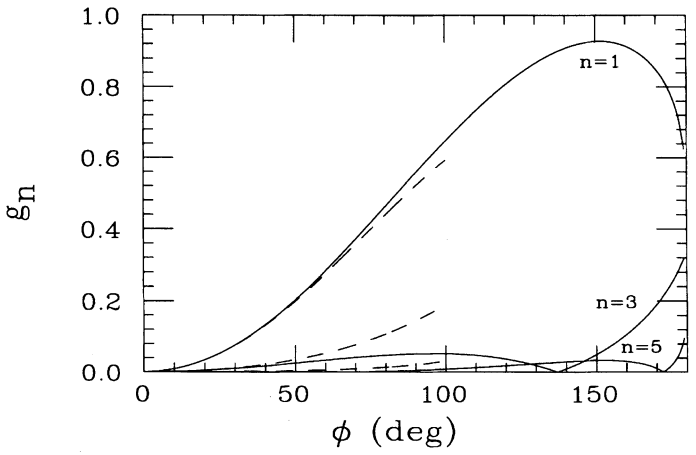


FIGURE 2: The resonance strength parameter $|g_n|$ for $n$=1,3,5 as a function of the peak phase $\phi$=$\hat{\phi}$. The solid lines are obtained from the analytic formula and the dashed lines are from the small amplitude approximation.

$n = 1, 3, 5$ (solid line). We found that $g_1$ is maximum at $\hat{\phi} = 151°$ with $\hat{g}_1 = 0.9275$. All $g_n$ factors vanish at $\hat{\phi} = 180°$, i.e., on the separatrix of the Hamiltonian torus.

For small amplitude oscillations, one finds an approximate solution given by

$$g_{2l+1} \approx i\hat{\phi}^2 \frac{\pi^2}{2\sqrt{2}kK^2} \frac{q^{l+1/2}}{1+q^{2l+1}}(2l+1), \tag{3.13}$$

which is a good approximation to the analytic solution near the origin with $\hat{\phi} \leq 50°$ (see the dash-dotted lines in Figure 2). Since $\hat{\phi} \sim J^{1/3}$, we have $g_{2l+1} \sim (2l+1)J^{2/3}$ for all $l$.

### *3.3 The action and the sum rule theorem*

Using Parseval's theorem and the coordinate transformation $d\psi = \frac{\nu_s}{Q_s}\delta d\phi$, we obtain the following sum rule

$$J = \frac{\nu_s}{2\pi Q_s}\int_{-\pi}^{\pi} \delta^2 d\psi = \frac{\nu_s}{Q_s}\sum_{n=-\infty}^{\infty} |g_n|^2. \tag{3.14}$$

This sum rule is valid for similar dynamical systems, where the kinetic energy of a Hamiltonian is proportional to the square of the momentum variable. Using Eq. (3.12), we obtain

$$J = \frac{32Q_s}{\nu_s}\sum_{\ell=0}^{\infty} \frac{q^{2\ell+1}}{(1+q^{2\ell+1})^2}\cos^2\left[(2\ell+1)\frac{\pi u_0}{2K}\right]. \tag{3.15}$$

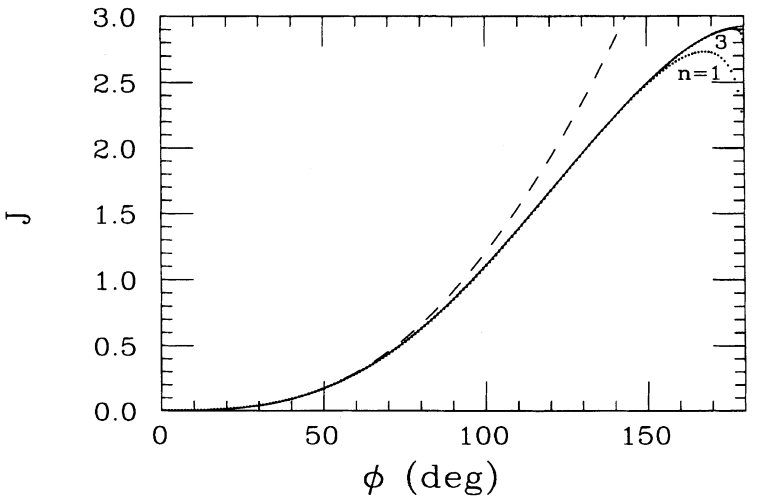


FIGURE 3: The action as a function of the peak phase $\phi=\hat{\phi}$. The solid line is obtained from the numerical integration, the dashed line is obtained from the small amplitude approximation, and dotted lines are from the sum rule with $g_1$ term and with $g_1, g_3$ terms.

The action, obtained from the numerical integration of Eq. (2.6) (solid line), is compared with that obtained from the small amplitude approximation of Eq. (2.17), shown as dashed line, in Fig. 3. The dotted lines are obtained from the sum rule of Eq. (3.15) with $g_1$ term only and with the $g_1$ and $g_3$ terms respectively. We find that the sum rule converges rapidly to the exact action. The action obtained by summing over $\ell = 0, 1, 2$ terms in Eq. (3.15) is effectively indistinguishable from the exact result up to $\hat{\phi} = 179°$.

As the sum rule converges more rapidly, a dynamical system is less likely to be disturbed by a phase modulation at high frequencies. Measurements of low order synchrotron modes can be used to set a limit on the instabilities of high order synchrotron modes, or vice versa.

### *3.4 Resonance island and bifurcation*

To verify the parametric resonance analysis of last section, we carried out numerical simulations based on the difference equations,

$$\begin{aligned} \phi_{n+1} &= \phi_n + 2\pi\delta_n + 2\pi\nu_m a\cos 2\pi n\nu_m, \\ \delta_{n+1} &= \delta_n - 2\pi\nu_s(\sin\phi_{n+1} - r\sin 2\phi_{n+1}) - \lambda\delta_n. \end{aligned} \tag{3.16}$$

For studying resonances, we do not include the damping effect, and we use the parameters $a = 2.5°$ and $\nu_s = 8 \times 10^{-4}$. The Poincaré surfaces of section are obtained by plotting one point every $N_m = \frac{1}{\nu_m}$ revolutions. Such *stroboscopic* maps will eliminate most of the less interesting time dependent term $\Delta\mathcal{H}$ of Eq. (3.9) and leave the true stochasticity in the Poincaré map for data analysis.

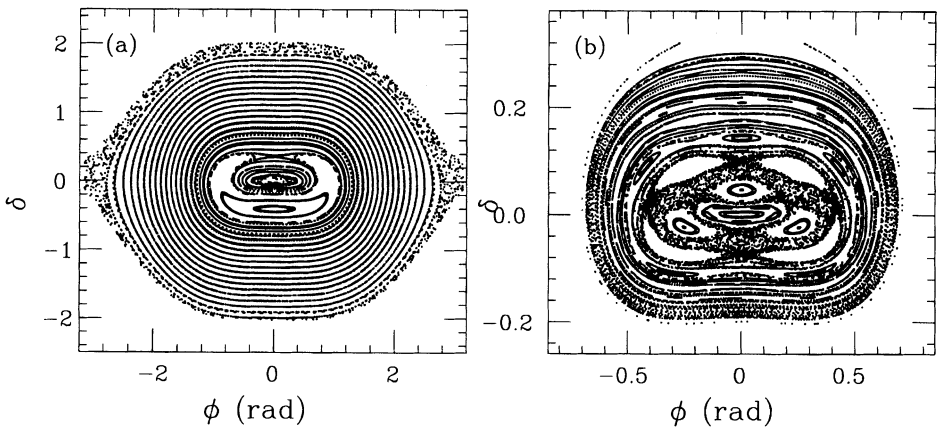


FIGURE 4: (a) Poincaré surfaces of section with $\nu_s = 8\times10^{-4}$, $\frac{\nu_m}{\nu_s}=0.5$, $a=2.5°$, and $r=0.5$. (b) The magnified center region showing 5:1, 3:1, 4:2 and 5:3 resonances and stochasticity due to the overlapping of 3:1 and 4:2 resonances.

Figure 4 displays the Poincaré surfaces of section at phase modulation tune $\nu_m = 0.5\nu_s$. A single resonance island in small amplitude region arises from the 1:1 parametric resonance. There is another small 1:1 island near the top of the rf bucket inside the stochastic sea. Although the modulation tune is smaller than the synchrotron tune, higher order resonances co-exist near the origin and the boundary of the rf bucket.

The locations of these resonances can be obtained from the intercepts of a horizontal line $\nu_m = 0.5\nu_s$ in Figure 1 with resonance lines $xQ_s$, where $x$ are integers or fractional numbers. The intercepts are located in phase space regions near the origin and the bucket boundary. The stochasticity arises from the overlap of these resonances. In particular, the chaotic region near the origin exhibits a rich spectrum of resonance islands. Magnifying the chaotic region near the origin, shown in Figure 4b, one observes that $n = 3, 5$ resonances lie closest to the origin while other fractional resonances with $x = \frac{4}{2}, \frac{5}{3}$, and $\frac{6}{4}$ are evident. These fractional resonances can result from higher order perturbations created by combining neighboring harmonics. The stochasticity has resulted from many overlapping resonances according to the Chirikov criterion. When the modulation amplitude is reduced to $a < 1°$, those higher order resonances become too weak to be seen, however $n = 3, 5$ resonances remain to be important.

Another example shown in Figure 5a for $\nu_m = 2.3\nu_s$ exhibits a dominant 3:1 resonance. Near the bucket boundary, the $\frac{8}{2}Q_s$ resonance due to the second order perturbation by combining 5:1 and 3:1 resonances is just barely recognizable. When the modulation tune is increased, the inner islands are observed to move outward and the outer islands move inward. At $\nu_m = 2.32\nu_s$, the inner 3:1 UFPs coincide with the outer 3:1 SFPs shown in Figure 5b. At this point, the inner 3:1 islands remain intact. When the modulation tune is increased to $\nu_m = 2.35\nu_s$, the third harmonic resonance islands disappear completely and

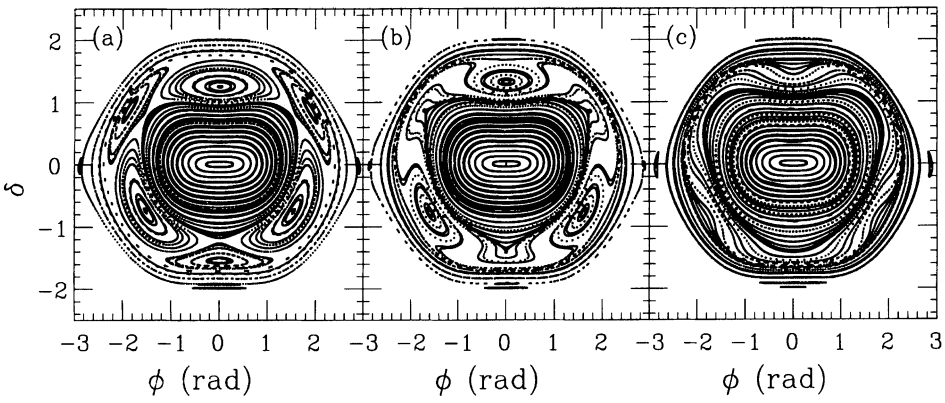


FIGURE 5: Near the 3rd harmonic resonance with $\nu_s = 8\times10^{-4}$, $a=2.5°$, and $r=0.5$. In (a), two 3:1 resonances merge toward each other at $\frac{\nu_m}{\nu_s}=2.3$. In (b), the UFPs of the inner island bifurcate with the SFP of the outer island at $\frac{\nu_m}{\nu_s}=2.32$. In (c), the 3:1 resonance disappears at $\nu_m \geq 2.35\nu_s$, and the outer secondary 8:2 resonance begins its journey inward.

the size of the secondary 8:2 resonance island is increased. This phenomenon is called a bifurcation, and the point where the UFPs and SFPs of the resonance island pairs merge together, is called a bifurcation point.

The bifurcation is systematically studied by mapping the SFP and the UFP of the bifurcation pair. Figure 6 shows the tree of bifurcation branches for resonances up to $n = 5$ by measuring the energy of the SFPs. The bifurcation tree would be extended to higher harmonics if the modulation tune is increased further. But as the resonance harmonic, $n$, increases, the strength function $g_n$ becomes smaller as shown in Figure 2, and thus the island structure may become invisible. In Figure 6, 1:1, 3:1, and 5:1 resonances are the primary parametric resonances, and 4:2 and 8:2 resonances are the secondary resonances. The solid lines are $\nu_m = xQ_s$ with $x = 1, \frac{4}{2}, 3, \cdots$. The bifurcation of SFPs and UFPs occurs near the top of the $\nu_m = xQ_s$ curve where the maximum energy is $E = 1.057\nu_s$, and the unperturbed tune at this point is $\hat{Q}_s = 0.7786\nu_s$. Starting from a small modulation tune and increasing it upward, resonance islands originated from the origin and the separatrix move toward the phase space point corresponding to $E = 1.057\nu_s$. When the modulation tune exceeds the maximum of a resonance branch $xQ_s$, the resonance structure vanishes. Thus the response of an external phase modulation reveals the basic frequency spectrum of the unperturbed Hamiltonian system.

Although the 4:2 resonance apparently has 4 islands, shown in Figure 4b, it differs from 4:1 resonance by the fact that a single Poincaré surface of section, by plotting the particle trajectory once every $\frac{1}{\nu_m}$ revolutions, traces only two islands, while the Poincaré surfaces of section for the 4:1 resonance will trace all four islands.

Since the characteristic tune of a double rf system with $r > 0.5$ has two peaks (see Figure 1), it would be interesting to examine the resonance overlapping criterion by performing numerical simulations. Figure 7 shows the Poincaré surfaces of section

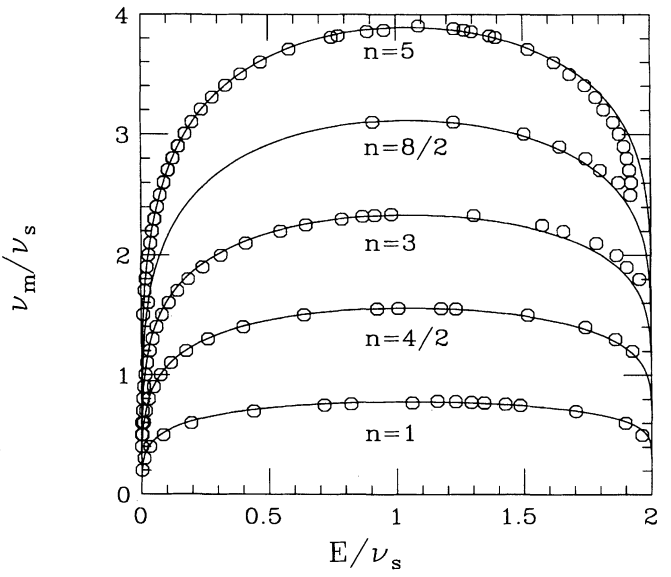


FIGURE 6: The rf phase modulation tune vs. the energies of SFPs for 1:1, 4:2, 3:1, 8:2, and 5:1 resonances are shown as circles, which are obtained from numerical simulations with $\nu_s=8\times10^{-4}$, $a=2.5°$ and $r=0.5$. The tree of bifurcation branches is compared with fractional multiples of the unperturbed synchrotron tune, shown as solid lines.

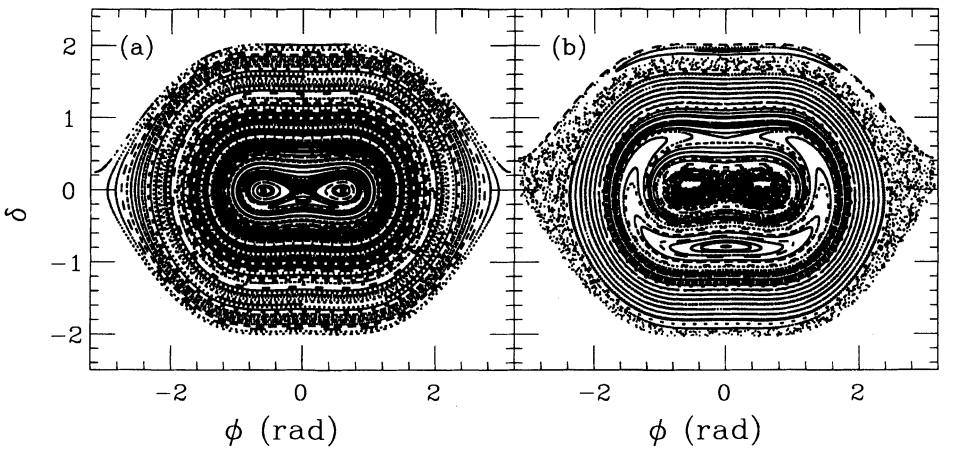


FIGURE 7: The Poincaré surfaces of section obtained from the numerical simulations with $\nu_s=8\times10^{-4}$, $a=2.5°$ and $r=0.6$. In (a), $\frac{\nu_m}{\nu_s}=0.3$, and in (b), $\frac{\nu_m}{\nu_s}=0.6055$.

obtained from numerical tracking at $r = 0.6$ with a modulation amplitude $a = 2.5°$ and $\nu_s = 8 \times 10^{-4}$. The example with $\nu_m = 0.3\nu_s$ is shown in Figure 7a, where the complicated Poincaré surfaces of section can be understood easily by draw a horizontal line of $\nu_m = 0.3\nu_s$ in Figure 1. This horizontal modulation line cuts through the synchrotron tune for $r = 0.6$ at 4 phase space locations. The inner buckets near the origin appear as two small islands surrounded by stochastic sea, which corresponds to the separatrix of inner buckets. At the center of each inner bucket, there is a 1:1 resonance visible in Figure 7a. This stochastic sea of the inner separatrix arises from the $\nu_m = 0.3\nu_s$ line cutting through the inner peak and its rational multiples of the synchrotron tune shown in Figure 1.

The island with the SFP located on the $\delta$ axis corresponds to the 1:1 parametric resonance that the line $\nu_m = 0.3\nu_s$ intersects the outer peak of the synchrotron tune. As the modulation tune increases, the width of the stochastic layer at the center region becomes wider, the inner 1:1 island moves outward, and the chaotic layer near the top of the rf bucket is also getting wider. When the resonance tune exceeds $\nu_m = 0.6055\nu_s$ as shown in Figure 7b, the outer 1:1 resonance island of the outer peak is visibly embedded in the stochastic sea of the bucket separatrix.

### 3.5 *Mechanism for higher order resonances*

We have found that the secondary parametric resonances, generated by neighboring harmonics, contribute significantly to the stochasticity in the Poincaré surfaces of section (see Figure 4b and Reference 9). Here, we discuss the mechanism for the secondary parametric resonances based on the canonical perturbation method.

We consider the case that $n_2 Q_s(J) \leq \nu_m \leq n_1 Q_s(J)$, where the Hamiltonian of Eq. (3.5) is dominated by $n_1$:1 and $n_2$:1 resonances and can be approximated by

$$\begin{aligned} H \approx\ & E(J) + a\nu_m \left[ |g_{n_1}(J)| \cos(n_1\psi - \nu_m\theta + \chi_{n_1}) \right. \\ & \left. + |g_{n_2}(J)| \cos(n_2\psi - \nu_m\theta + \chi_{n_2}) \right], \end{aligned} \tag{3.17}$$

where $n_1$ and $n_2$ are neighboring harmonics. Using the generating function

$$\begin{aligned} W_2(\psi, \bar{J}) =\ & \psi\bar{J} + F_{n_1}(\bar{J}) \sin(n_1\psi - \nu_m\theta + \chi_{n_1}) \\ & + F_{n_2}(\bar{J}) \sin(n_2\psi - \nu_m\theta + \chi_{n_2}), \end{aligned} \tag{3.18}$$

the new action-angle variables $(\bar{\psi}, \bar{J})$ are related to $(\psi, J)$ by

$$\begin{aligned} J &= \bar{J} + n_1 F_{n_1}(\bar{J}) \cos(n_1\psi - \nu_m\theta + \chi_{n_1}) + n_2 F_{n_2}(\bar{J}) \cos(n_2\psi - \nu_m\theta + \chi_{n_2}), \\ \bar{\psi} &= \psi + F'_{n_1}(\bar{J}) \sin(n_1\psi - \nu_m\theta + \chi_{n_1}) + F'_{n_2}(\bar{J}) \sin(n_2\psi - \nu_m\theta + \chi_{n_2}). \end{aligned} \tag{3.19}$$

The new Hamiltonian becomes

$$\begin{aligned}\bar{H} &= E(\bar{J}) + [(n_1 Q_s - \nu_m) F_{n_1} + a\nu_m |g_{n_1}(\bar{J})|] \cos(n_1 \bar{\psi} - \nu_m \theta + \chi_{n_1}) \\ &+ [(n_2 Q_s - \nu_m) F_{n_2} + a\nu_m |g_{n_2}(\bar{J})|] \cos(n_2 \bar{\psi} - \nu_m \theta + \chi_{n_2})] \\ &+ \frac{1}{2} \frac{\partial Q_s}{\partial \bar{J}} [n_1 F_{n_1} \cos(n_1 \bar{\psi} - \nu_m \theta + \chi_{n_1}) + n_2 F_{n_2} \cos(n_2 \bar{\psi} - \nu_m \theta + \chi_{n_2})]^2 \\ &+ a\nu_m \left[ \frac{\partial |g_{n_1}|}{\partial \bar{J}} \cos(n_1 \bar{\psi} - \nu_m \theta + \chi_{n_1}) + \frac{\partial |g_{n_2}|}{\partial \bar{J}} \cos(n_2 \bar{\psi} - \nu_m \theta + \chi_{n_2}) \right] \\ &\times [n_1 F_{n_1} \cos(n_1 \bar{\psi} - \nu_m \theta + \chi_{n_1}) + n_2 F_{n_2} \cos(n_2 \bar{\psi} - \nu_m \theta + \chi_{n_2})], \end{aligned} \tag{3.20}$$

where we used $\psi \approx \bar{\psi}$. By setting $F_{n_1} = -\frac{a\nu_m |g_{n_1}(\bar{J})|}{n_1 Q_s - \nu_m}$ and $F_{n_2} = -\frac{a\nu_m |g_{n_2}(\bar{J})|}{n_2 Q_s - \nu_m}$, the Hamiltonian due to the second order perturbation becomes,

$$\begin{aligned}\bar{H} &= E(\bar{J}) + \left( \frac{1}{2} \frac{\partial Q_s}{\partial \bar{J}} n_1^2 F_{n_1}^2 + a\nu_m \frac{\partial |g_{n_1}|}{\partial \bar{J}} n_1 F_{n_1} \right) \cos^2(n_1 \bar{\psi} - \nu_m \theta + \chi_{n_1}) \\ &+ \left( \frac{1}{2} \frac{\partial Q_s}{\partial \bar{J}} n_2^2 F_{n_2}^2 + a\nu_m \frac{\partial |g_{n_2}|}{\partial \bar{J}} n_2 F_{n_2} \right) \cos^2(n_2 \bar{\psi} - \nu_m \theta + \chi_{n_2}) \\ &+ \left( \frac{\partial Q_s}{\partial \bar{J}} n_1 n_2 F_{n_1} F_{n_2} + a\nu_m \frac{\partial |g_{n_1}|}{\partial \bar{J}} n_2 F_{n_2} + a\nu_m \frac{\partial |g_{n_2}|}{\partial \bar{J}} n_1 F_{n_1} \right) \\ &\times \cos(n_1 \bar{\psi} - \nu_m \theta + \chi_{n_1}) \cos(n_2 \bar{\psi} - \nu_m \theta + \chi_{n_2}). \end{aligned} \tag{3.21}$$

Near the resonance condition at $\nu_m \approx \frac{1}{2}(n_1 + n_2) Q_s(J)$, the Hamiltonian can be approximated by

$$\bar{H} \approx E(\bar{J}) + \tilde{g}_{(n_1+n_2)} \cos[(n_1 + n_2)\bar{\psi} - 2\nu_m \theta + (\chi_{n_1} + \chi_{n_2})], \tag{3.22}$$

where

$$\tilde{g}_{(n_1+n_2)} = \frac{1}{2} \frac{\partial Q_s}{\partial \bar{J}} n_1 n_2 F_{n_1} F_{n_2} + \frac{a\nu_m}{2} \frac{\partial |g_{n_1}|}{\partial \bar{J}} n_2 F_{n_2} + \frac{a\nu_m}{2} \frac{\partial |g_{n_2}|}{\partial \bar{J}} n_1 F_{n_1}$$

is the resonance strength for the secondary $(n_1 + n_2) : 2$ resonance. These higher order resonances are responsible for the stochasticity shown in Figure 4b.

### *3.6 Attractor and beam splitting*

The synchrotron motion for a single rf system has been well studied.[11] When the rf system is subject to a phase modulation, or the field of a dipole in a high dispersion region is modulated, the beam was observed to split into beamlets, which were identified unambiguously as

attractors associated with parametric resonances due to an external phase modulation, or the synchro-betatron coupling due to a dipole field modulation. Here we investigate the attractors arising from the phase modulation of a double rf system.

To examine the incoherent particle damping path, we numerically study basins of attraction using Eq. (3.16) with parameters $\nu_s = 8 \times 10^{-4}$ and $a = 2.5°$. The damping parameter is given by $\lambda = \frac{2\alpha}{f_0}$ with the revolution frequency $f_0 = 1.03168$ MHz and the damping rate measured to be about $\alpha = (3 \pm 1)s^{-1}$ for large amplitude synchrotron oscillations at the IUCF cooler ring.[11]

Numerical simulations of multi-particle are performed near the 1:1 resonance. The phase space is rotated a 90° so that the SFP of the 1:1 resonance lies on the $\phi$ axis. With phase space damping, these SFPs become attractors. The basins of attraction depend on the damping rate, modulation frequency and amplitude, and initial particle coordinates. Figure 8a shows the final beam distribution for $\nu_m = 0.6\nu_s$ and $\alpha = 4\ \mathrm{s}^{-1}$, where $200 \times 200$ particles are initially distributed uniformly in a grid of $\phi \in [-\pi, \pi]$ and $\delta \in [-2, 2]$. Each particle is tracked for 416, 600 revolutions, and its initial coordinates are numbered according to the attractor location. In this case, most of these particles damp to the inner 1:1 attractor and the center attractor. A small portion of particles damp to the outer 1:1 attractor. We also note that the outer 1:1 attractor is off $\phi$ axis. This is because the damping force breaks the symmetry of the Hamiltonian system. By identifying each particle with its attractor, initial phase space coordinates which converge to the inner 1:1 attractor are shown as black dots in Figure 8b. The basins of attraction form non-intersecting interweaving rings. The complementary phase space converges mainly toward the center region. A small blank region on the right side of initial phase space damp to the outer 1:1 attractor.

## 4 VOLTAGE MODULATION

The voltage modulation is also important since it is related to rf noises, power supply ripple, and wake fields, etc. A careful theoretical study is beneficial to understand coherent beam instabilities. Hamilton's equations of motion with a sinusoidal voltage modulation are given by

$$\begin{aligned} \dot{\phi} &= \nu_s \delta, \\ \dot{\delta} &= -\nu_s (1 + \epsilon \sin \nu_m \theta)(\sin \phi - r \sin 2\phi) \end{aligned} \tag{4.1}$$

where $\epsilon = \frac{V_m}{V_0}$. Here $V_m$ and $\nu_m$ are the voltage modulation amplitude and tune. The Hamiltonian becomes

$$\begin{aligned} H &= \frac{1}{2}\nu_s \delta^2 + \nu_s (1 + \epsilon \sin \nu_m \theta)\left[(1 - \cos\phi) - \frac{r}{2}(1 - \cos 2\phi)\right] \\ &= (1 + \epsilon \cos \nu_m \theta) E - \frac{1}{2}\epsilon \nu_s \delta^2 \cos \nu_m \theta, \end{aligned} \tag{4.2}$$

where $E$ is the energy of the unperturbed Hamiltonian.

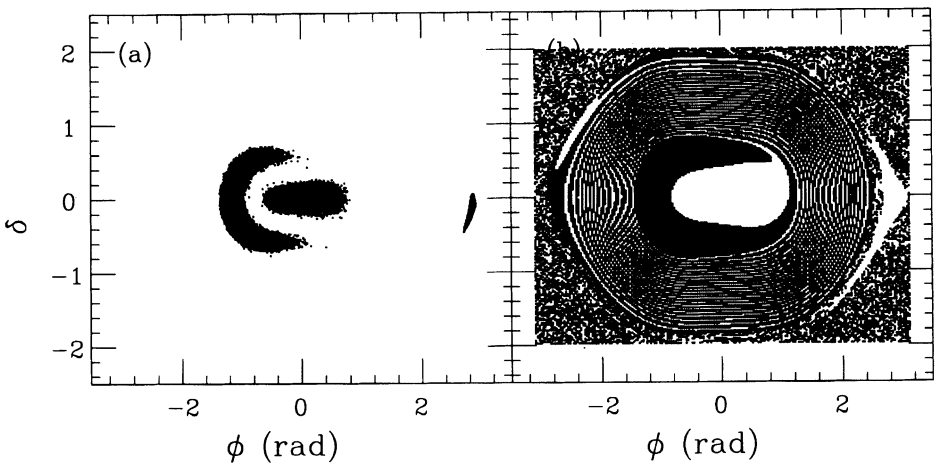


FIGURE 8: In (a), the phase space distribution of 200×200 particles after tracking 416600 revolutions is shown with $\alpha$=4 $s^{-1}$, $\nu_s$=8×10$^{-4}$, $\frac{\nu_m}{\nu_s}$=0.6, $r$=0.5, and $a$=2.5°. In (b), the dots, showing initial phase space points, converge toward the inner 1:1 attractor, while the complementary region in the phase space converges mainly toward the center region, and a small patch on the right side, left blank, converges to outer 1:1 island.

### *4.1 Resonance strength function*

In the analysis of parametric resonances due to the time dependent phase modulation, we expand the momentum variable $\delta$ into a Fourier series and find that only odd harmonics are nonzero. For the voltage modulation, the perturbation potential in Eq. (4.2) can also be expanded in the action-angle variables of the unperturbed Hamiltonian with

$$\delta^2 = \sum_{n=-\infty}^{\infty} G_n(J) e^{in\psi}, \tag{4.3}$$

where $G_n(J)$ is given by

$$G_n(J) = \frac{1}{2\pi} \int_{-\pi}^{\pi} \delta^2 e^{-in\psi} d\psi, \tag{4.4}$$

with $G_{-n} = G_n^*$. Using Eqs. (3.3) and (3.4), we obtain

$$G_n(J) = \sum_{l=-\infty}^{\infty} g_l(J) g_{n-l}(J), \tag{4.5}$$

Since $g_n$, given in Eq. (3.12), contains only odd harmonics, the factor $G_n$ is not zero only for even harmonics.

Since the zeroth harmonic of the voltage modulation is the average of the potential energy and the sum of the square of the phase modulation strengths is related to the kinetic energy, the sum rule for a conservation of total energy is given by

$$G_0 = \sum_{n=-\infty}^{\infty} |g_n|^2 = \frac{Q_s}{\nu_s} J, \tag{4.6}$$

where the latter equality is obtained from the sum rule in Section 3.3. The sum rule for the strength function $G_n$ of the voltage modulation is given by

$$\sum_{n=-\infty}^{\infty} |G_n|^2 = \frac{Q_s}{\pi \nu_s} \int_{-\hat{\phi}}^{\hat{\phi}} \delta^3 d\phi, \tag{4.7}$$

which can be expressed as a sum of elliptical integrals of the first kind, the third kind, and their derivatives.

Using Eq. (4.5), we obtain

$$G_2(I) = g_1^2 + \sum_{n \neq 1} g_{-n+2} g_n. \tag{4.8}$$

Thus the 2:1 resonance strength function for voltage modulation is roughly proportional to the square of the 1:1 phase modulation strength, i.e. $G_2 \approx g_1^2$, which is a good approximation up to $\hat{\phi} = 120°$. The analytic solution for $G_n$, obtained in Appendix C, is

$$G_n = \frac{4KQ_s^2}{\pi \nu_s^2} \frac{q^{n/2}}{1-q^n} \left[ \sqrt{2} \frac{\sin \frac{n\pi u_0}{2K}}{\sin \frac{\hat{\phi}}{2}} + \frac{n\pi}{K} \cos\left(\frac{n\pi u_0}{2K}\right) \right] \cos \frac{n\pi}{2}, \tag{4.9}$$

where $K$ and $u_0 = F\left(\arccos\left(\frac{\sqrt{k^2 - \frac{1}{2}}}{k}\right), k\right)$ are respectively the complete and the incomplete elliptical function of the first kind with modulus $k = \sqrt{\frac{1}{2}(1 + \sin^2 \frac{\hat{\phi}}{2})}$, and $q = e^{-\pi K'/K}$. Note that the $G_0$ can be obtained from the sum rule of Eq. (4.6). Figure 9 shows $|G_n|$ as a function of $\hat{\phi}$.

### 4.2 *Analysis of parametric resonances*

The Hamiltonian, expressed in terms of $(J, \psi)$, becomes

$$\begin{aligned} H \;=\; & E(J) + \epsilon E(J) \cos \nu_m \theta - \frac{1}{2} \epsilon \nu_s \sum_{n \geq 0} |G_n(J)| [\cos(n\psi - \nu_m \theta + \chi_n) \\ & + \cos(n\psi + \nu_m \theta + \chi_n)]. \end{aligned} \tag{4.10}$$

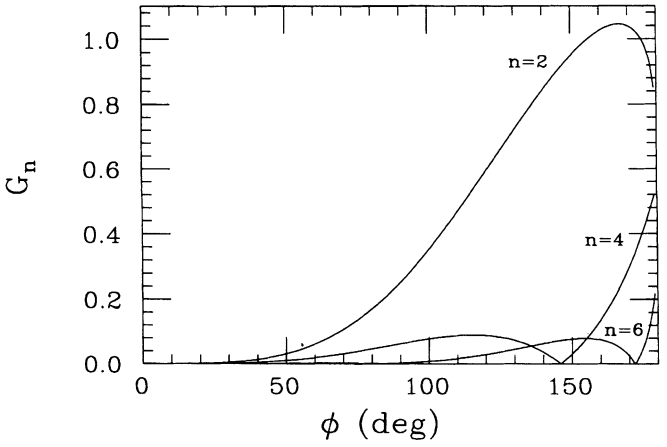


FIGURE 9: The resonance strength parameter $G_n$ for voltage modulation obtained from analytic formula is shown as a function of the maximum phase oscillation amplitude.

where $\chi_n$ is the phase of $G_n(J)$. If the modulation tune $\nu_m$ is close to one of the parametric resonances, e.g., $\nu_m \approx n\dot{\psi}$, then the resonance term contributes coherently to perturb particle motion. We transform the Hamiltonian to a resonance rotating frame by using the generating function,

$$W_2(\psi, I) = (\psi - \frac{\nu_m}{n}\theta + \frac{\chi_n}{n})I. \tag{4.11}$$

The new action angle variables are given by

$$J = I, \quad \text{and} \quad \gamma = \psi - \frac{\nu_m}{n}\theta + \frac{\chi_n}{n}, \tag{4.12}$$

and the new Hamiltonian becomes

$$\mathcal{H} = E - \frac{\nu_m}{n}I - \frac{1}{2}\epsilon\nu_s|G_n|\cos n\gamma + \Delta\mathcal{H}(I, \gamma, \theta), \tag{4.13}$$

where the time dependent part is given by

$$\begin{aligned}\Delta\mathcal{H} = {} & \epsilon[E(I) - Q_s I]\cos\nu_m\theta - \frac{1}{2}\epsilon\nu_s|G_n|\cos(n\gamma + 2\nu_m\theta) \\ & - \frac{1}{2}\epsilon\nu_s \sum_{\ell\geq 2, \ell\neq n} |G_\ell| \left[\cos\left[\ell\gamma + \left(\frac{\ell}{n} - 1\right)\nu_m\theta + \chi_\ell - \frac{\ell}{n}\chi_n\right]\right. \\ & \left. + \cos\left[\ell\gamma + \left(\frac{\ell}{n} + 1\right)\nu_m\theta + \chi_\ell - \frac{\ell}{n}\chi_n\right]\right].\end{aligned} \tag{4.14}$$

Since the time dependent part $\Delta\mathcal{H}$, proportional to $\epsilon$, contributes incoherently to particle motion, it constitutes a small perturbation to the Hamiltonian flow. The time averaged $n$:1 resonance Hamiltonian is

$$\mathcal{H} = E(I) - \frac{\nu_m}{n} I - \frac{1}{2}\epsilon\nu_s |G_n| \cos n\gamma. \tag{4.15}$$

The fixed points of the time averaged Hamiltonian are given by

$$n\gamma_{\mathrm{FP}} = l\pi, \quad (l = 0, 1, 2, 3...), \tag{4.16}$$

$$Q_s(I_{\mathrm{FP}}) - \frac{\nu_m}{n} \pm \frac{1}{2}\epsilon\nu_s |G_n'(I_{\mathrm{FP}})| = 0,$$

where ($\gamma_{\mathrm{FP}}$, $I_{\mathrm{FP}}$) are phase space coordinates of fixed points, $G_n'$ is the derivative of strength function. For a small perturbation with $\epsilon \ll 1$, the resonance condition of Eq. (4.16) is approximately given by $\nu_m \approx nQ_s$, where $n$ is an even number.

### 4.3 *Resonance islands and bifurcation*

To confirm the existence of resonance islands discussed in Section 4.2, we perform numerical simulations for the following difference equations

$$\begin{aligned} \phi_{n+1} &= \phi_n + 2\pi\nu_s\delta_n, \\ \delta_{n+1} &= \delta_n - 2\pi\nu_s(1 + \epsilon\sin 2\pi n\nu_m)[\sin\phi_{n+1} - r\sin 2\phi_{n+1}] - \lambda\delta_n, \end{aligned} \tag{4.17}$$

with parameters $\epsilon = 0.05$, $\nu_s = 8 \times 10^{-4}$, and the phase damping parameter $\lambda = 0$. The modulation tune $\nu_m$ is varied. Figure 10a shows Poincaré surfaces of section with $\nu_m = 0.75\nu_s$, which is close to $\hat{Q}_s$. We note that there are two pairs of islands due to the second order 2:2 resonance with SFPs located on $\delta$ and $\phi$ axes respectively. The 2:2 resonance differs from the 2:1 ($n = 2$) resonance because it bifurcates at $\nu_m = \hat{Q}_s$.

Near the boundary of the rf bucket, the chaotic layer arises from many overlapping resonances, where many parametric resonances collapse in a small region of the phase space with sizable strength functions. However, there is no stochasticity observed near the center region, where many higher order resonances overlap. The magnified center region, shown in Figure 10b, exhibits only $n = 2$, 4 and 6 resonances. This can be understood from the second order perturbation theory discussed in Section 3.5. Since $G_n(I)$ of Eq. (4.5) depends on a higher power of action than that of $g_n(I)$ (see also Figure 9), second order perturbation for voltage modulation is less important than for phase modulation when the oscillation amplitudes are small.

To study the bifurcation of the 2:1 resonance, numerical simulations are performed by varying the modulation tune near $n = 2$ resonance. Figure 11a shows Poincaré surfaces of section for $\nu_m = 1.3\nu_s$ with $\epsilon = 0.05$, where the inner and the outer 2:1 islands appear as pairs. Here, the outer 2:1 islands are still embedded in the chaotic region. When the modulation tune is increased, inner islands move outward and outer islands move inward, and stochastic layer width increases. Some visible tertiary islands surrounding the outer 2:1

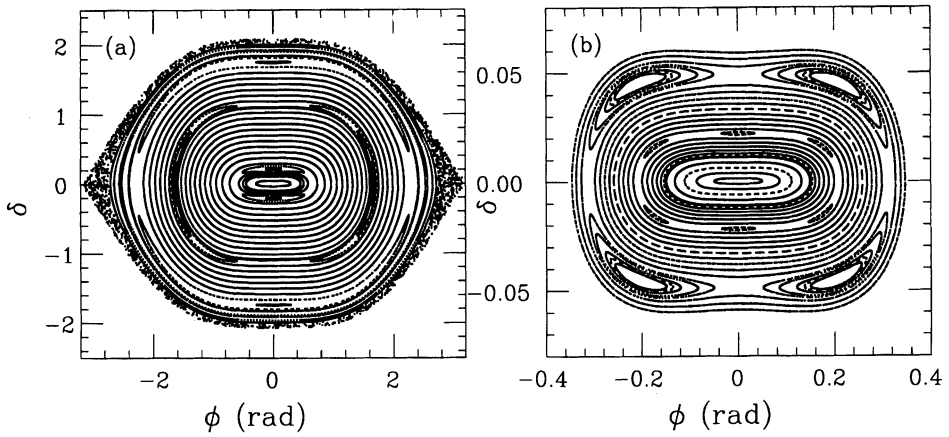


FIGURE 10: Poincaré surfaces of section obtained from numerical simulations for voltage modulation with $\nu_s = 8\times10^{-4}$, $\frac{\nu_m}{\nu_s} = 0.75$, $\epsilon = 0.05$, and $r = 0.5$. In (a), the inner 2:1 primary resonance and two 2:2 secondary bifurcation pairs can be observed, and in (b), the center region is magnified to exhibit the primary 4:1 and 6:1 resonances.

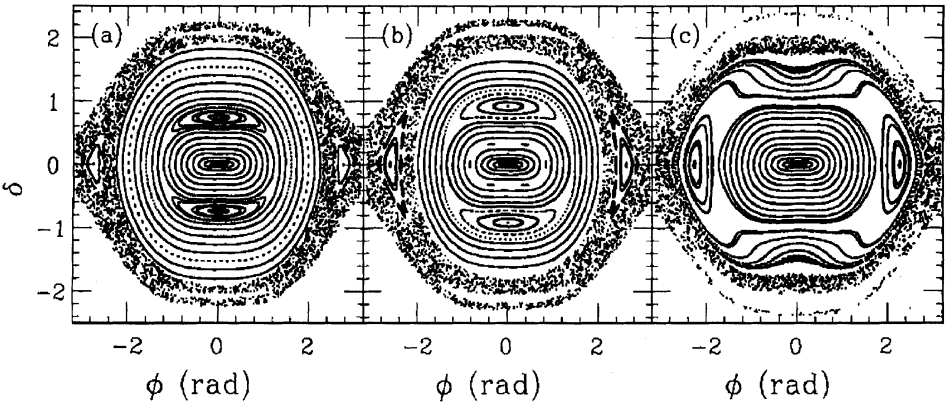


FIGURE 11: Poincaré surfaces of section obtained from numerical simulations for voltage modulation with $\nu_s = 8\times10^{-4}$, $\epsilon = 0.05$, and $r = 0.5$ are shown in (a) $\frac{\nu_m}{\nu_s} = 1.3$, (b) $\frac{\nu_m}{\nu_s} = 1.4$ and (c) $\frac{\nu_m}{\nu_s} = 1.55$ respectively. In (c), the bifurcation between the inner 2:1 SFPs and the outer 2:1 UFPs pairs has just occurred.

islands are visible in Figure 11b, where $\nu_m = 1.4\nu_s$. To analyze these tertiary islands, one has to expand the Hamiltonian of Eq. (4.15) in terms of "proper action" around the 2:1 SFP and include the dominant time dependent components from Eq. (4.14).

When the modulation tune reaches $\nu_m = 1.55\nu_s$, as shown in Figure 11c, SFPs of inner islands and UFPs of outer islands have merged, and the inner islands have just disappeared. In this example, the second harmonic resonance disappears completely at $\nu_m = 1.56\nu_s$. Similarly, 4:1 and 6:1 resonance bifurcations occur at $\nu_m \approx 3\nu_s$ and $\nu_m \approx 4.5\nu_s$.

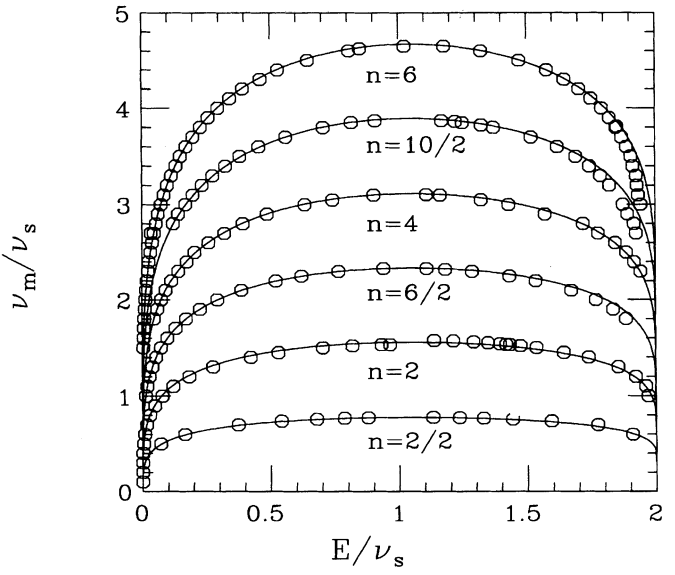


FIGURE 12: The voltage modulation tunes vs. energies of SFPs for 2:2, 2:1, 6:2, 4:1, 10:2, 6:1 resonances are shown as circles, which are obtained from numerical simulations with $\epsilon$=0.05, $\nu_s$=$8\times10^{-4}$, and $r$=0.5. The tree of bifurcation branches is compared with fractional multiples of the unperturbed synchrotron tune, shown as solid lines.

The bifurcation of parametric resonances are carefully studied by mapping the SFPs of inner and outer islands. By measuring the energy of SFPs, we obtain a tree of bifurcation branches for parametric resonances. Figure 12 plots the modulation tune vs. the energy of SFPs (circles) up to the 6th harmonic. Here the 2:1, 4:1, and 6:1 resonances are primary resonances, while the 2:2, 6:2 and 10:2 resonances arise from the second order perturbation by combining neighboring harmonics. We find that the tree of bifurcation branches follows the tune of the unperturbed Hamiltonian, shown as solid lines in Figure 12. Increasing the modulation tune from a lower value to a high value, SFPs and UFPs from different island pairs approach each other, and bifurcate at about $E/\nu_s = 1.057$ or $\hat{\phi} = 117°$.

Since the tune of a double rf system with $r > 0.5$ has double peaks, the bifurcation of this system will be complicated. The basic physics involved is similar to what has been discussed earlier in this section.

### *4.4 Attractor and beam splitting*

For a single rf cavity, the effect of rf voltage modulation on synchrotron motion was experimentally studied,[12] where experimental data revealed resonance structure and bifurcation of attractors. With electron cooling, beam particles were observed to damp incoherently toward SFPs of resonance islands in the resonance rotating frame. These beamlets were observed to rotate around the origin.

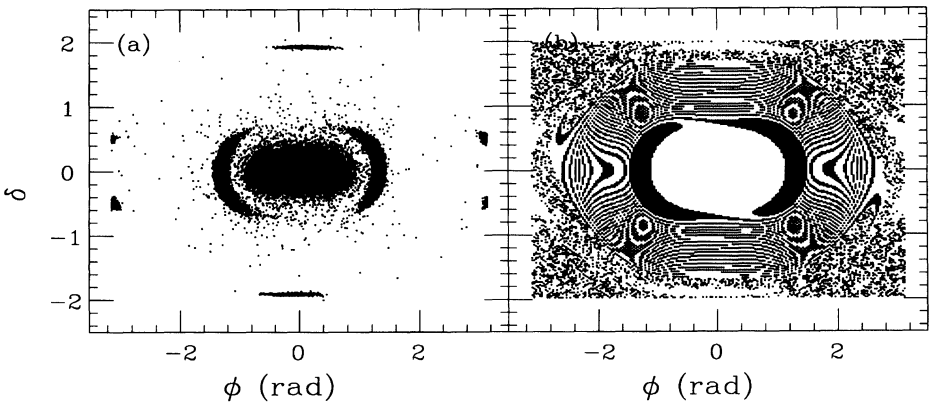


FIGURE 13: In (a), the final phase space distribution of 200×200 particles after tracking 192200 revolutions is shown with $\alpha$=4 $s^{-1}$, $\nu_s$=8×$10^{-4}$, $\frac{\nu_m}{\nu_s}$=1.3, $r$=0.5, and $\epsilon$=0.05. In (b), the dots, showing the initial phase space points, converge toward the inner 2:1 attractors, while the complementary phase space points converge mainly toward the center region, and those small patches, left blank, converge to the outer 2:1 and higher order resonances.

For a double rf system with voltage modulation, we study the basin of attraction numerically by using the difference equations (4.17) with parameters $\nu_s = 8 \times 10^{-4}$ and $\epsilon = 0.05$. The resonance 2:1 at $\nu_m = 1.3\nu_s$ is examined with SFPs located on $\phi$ axis. The case $\alpha = 14\ s^{-1}$ is identical to Figure 11a with a 90° phase space rotation. The damping force is included in our numerical simulations, and beam particles are observed to damp incoherently toward SFPs. The attractor that a particle will damp to depends on the damping rate, the modulation amplitude and tune, and the initial phase space coordinates. Since there are several SFPs in the bucket, particles in a beam bunch may converge to different attractors and result in beam splitting.

The basins of attraction can be obtained from the damping path in multiparticle tracking. Figure 13a shows the final distribution of such numerical simulations, where 200 × 200 particles are initially distributed uniformly in a grid of $\phi \in [-\pi, \pi]$ and $\delta \in [-2, 2]$ with parameters $\nu_s = 8 \times 10^{-4}$, $\nu_m = \frac{1}{961}$ and $\alpha = 4\ s^{-1}$. Particles are tracked for 192200 revolutions. In this case, most of these particles damp to the center region and the inner 2:1 attractors. Two small patches on $\delta$ axis correspond to the outer 2:1 attractors. These inner and outer 2:1 attractors form bifurcation pairs. A small portion of particles near the separatrix damp to an attractor of higher harmonic resonances. The basins of attraction for initial phase space coordinates are shown in Figure 31b, where dots are initial phase space coordinates which converge toward the inner 2:1 attractors, while the major portion of the complementary phase space coordinates damp toward the center attractor. Some small patches, left blank, converge toward various other attractors shown in Figure 13a.

## 5 CONCLUSION

In conclusion, we have systematically studied synchrotron motion for a double rf system with harmonic ratio $h = 2$. The synchrotron tune has been obtained analytically for different

voltage ratios. At the voltage ratio $r = V_2/V_1 = 0.5$, the synchrotron tune becomes zero at both the origin and the separatrix. For $r > 0.5$, the synchrotron tune becomes double-peaked, which reflects two inner buckets inside the rf bucket. Since $r = 0.5$ is preferable in most practical applications, we have obtained analytic formula in this case for the coordinate transformation from phase space coordinates $(\phi, \delta)$ to the action-angle variables $(J, \psi)$.

Using these analytic solutions, parametric resonance strength functions for rf phase or voltage modulation have been obtained. Sum rules for resonance strength functions have been derived. Using the rate of convergence of a sum rule, one can estimate the importance of high order synchrotron mode excitation. We find analytically that the rf phase modulation drives only odd harmonic synchrotron modes and the voltage modulation excites only even synchrotron modes. In numerical simulations, we have however observed many rational harmonics, which arise from higher order perturbation. Since all *fractional* multiples of the synchrotron tune collapse to zero at both the origin and the separatrix at the voltage ratio of $r = \frac{1}{2}$, overlapping parametric resonances cause chaos at the origin and the boundary of the rf bucket. The width of the stochastic layer depends on the modulation frequency and amplitude.

To understand the effects of parametric resonances on beam motion, we have systematically studied the dependence of SFPs and UFPs on modulation tune. The tree of bifurcation branches for these fixed points follows the intrinsic tune of the unperturbed Hamiltonian. With phase space damping due to electron or stochastic cooling, SFPs become attractors. Particles damp incoherently to these attractors, while these attractors precess coherently about the center of the rf bucket at the synchrotron tune $Q_s(I_{\mathrm{SFP}})$.

REFERENCES


1. D. Neuffer *et al.*, *Particle Accelerators*, **23**, 133 (1988).
2. R. Averill *et al.*, *Proc. 8th Int. Conf. on High Energy Accelerators*, CERN (1971) p. 301.
3. P. Bramham *et al.*, *Proc. 9th Int. Conf. on High Energy Accelerators*, CERN (1974); P. Bramham *et al.*, *IEEE Trans. Nucl. Sci.* **NS-24**, 1490 (1977).
4. The bunching factor $B_f$ is also defined as the ratio of the average current to the peak current.
5. J.M. Baillod *et al.*, *IEEE Trans. Nucl. Sci.* **NS-30**, 3499 (1983); G. Gelato *et al.*, *Proc. IEEE Part. Acc. Conf.*, Washington (1987), p. 1298.
6. The CE37C experiment logbook, accelerator physics group, at Indiana University. The experiment was carried out with a single bunch at a kinetic energy of 45 MeV. The cycle time was about 10 second, where the injected beam was electron cooled for 3 seconds. A bunching factor (BF) of 0.3 in a double rf system was obtained instead of a BF of 0.05 in an equivalent single rf system.
7. A. Hofmann and S. Myers, *Proc. 11th Int. Conf. on High Energy Accelerators*, CERN (1980), p. 610.
8. J. Wei, *Proc. of the third European Part. Accel. Conf.*, France, p. 833,(1992); A. Pauluhn, DESY lab report, HERA 93–02 (1993).
9. S.Y. Lee *et al.*, *Phys. Rev. E*, **49**, 5717 (1994).
10. I.S. Gradshteyn and I.M. Ryzlik, *Table of Integrals, Series, and Products*, (Academic Press, New York, 1980); E.T. Whittaker and G.N. Watson, *A Course of Modern Analysis*, 4th edition, pp. 404–427 (Cambridge Univ. Press, 1962).
11. M. Ellison *et al.*, *Phys. Rev. Lett.*, **70**, 591 (1993); M. Syphers *et al.*, *Phys. Rev. Lett.*, **71**, 719 (1993); H. Huang *et al.*, *Phys. Rev. E*, **48**, 4678 (1993); Y. Wang *et al.*, *Phys. Rev. E*, **49**, 1610 (1994).
12. D. Li *et al.*, *Phys. Rev.* E, **48**, R1638 (1993).

## APPENDIX A: THE SYNCHROTRON TUNE

The Hamiltonian equation for a double rf system with $h = 2$ is given by

$$H = \frac{1}{2}\nu_s\delta^2 + \nu_s\left[(1-\cos\phi) - \frac{r}{2}(1-\cos 2\phi)\right], \tag{A1}$$

where $\nu_s$ is the synchrotron tune of the primary rf system, $r = \frac{V_2}{V_1}$ is the voltage ratio of two rf cavities. For a given energy $E$, the action variable is given by

$$J(E) = \frac{1}{2\pi}\oint \delta d\phi = \frac{1}{\pi}\int_{-\hat{\phi}}^{\hat{\phi}} \delta d\phi, \tag{A2}$$

and the synchrotron tune is then given by $Q_s = (\frac{\partial J}{\partial E})^{-1}$. Two cases are discussed below:

### *Appendix A1: The $r \leq 0.5$ Case*

Making a change of variables using $t = \tan\frac{\phi}{2}$, $d\phi = \frac{2dt}{1+t^2}$, $t_0 = \tan\frac{\hat{\phi}}{2}$, and $\tau = t/t_0$, we obtain

$$\frac{\partial J}{\partial E} = \frac{2\left(1+t_0^2\right)}{\pi\nu_s t_0\left[1+(1+2r)t_0^2\right]^{1/2}}\int_0^1 \frac{d\tau}{\left\{(1-\tau^2)\left(\frac{1-2r+t_0^2}{t_0^2[1+(1+2r)t_0^2]}+\tau^2\right)\right\}^{1/2}}. \tag{A3}$$

The synchrotron tune becomes[10]

$$\frac{Q_s}{\nu_s} = \frac{\pi\sqrt{(1-2r)+2t_0^2+(1+2r)t_0^4}}{2(1+t_0^2)K(k_1)}, \tag{A4}$$

where $K(k_1)$ is the complete elliptic integral of the first kind with the modulus

$$k_1 = \frac{t_0\sqrt{1+(1+2r)t_0^2}}{\sqrt{(1-2r)+2t_0^2+(1+2r)t_0^4}}. \tag{A5}$$

This formula is also valid for $r > 0.5$ and $\hat{\phi} > \phi_b$, where $\phi_b$ is the intercept of the inner separatrix with the phase axis.

### *Appendix A2: The $r > 0.5$ Case*

For $r > 0.5$, the origin of phase space $\delta = \phi = 0$ becomes a UFP of the unperturbed Hamiltonian. There are two SFPs located at $\delta = 0$ and $\phi = \pm\phi_f$ where $\cos\frac{\phi_f}{2} = \frac{1}{2r}$.

The inner separatrix, which passes through the origin, intersects the phase axis at $\pm\phi_b$ with $\cos\frac{\phi_b}{2} = \frac{1}{\sqrt{2r}}$.

A given torus inside the inner bucket corresponds to a Hamiltonian flow of constant Hamiltonian value. Let $\phi_l$ and $\phi_u$ be the lower and the upper intercepts of the torus with phase axis, i.e., $\phi_u = \hat{\phi}$ and $\sin\frac{\phi_l}{2} = \sqrt{\sin^2\frac{\phi_b}{2} - \sin^2\frac{\phi_l}{2}}$. The derivative of the action with respect to the energy for a torus becomes

$$\frac{\partial J}{\partial E} = \frac{\sqrt{(1+t_u^2)(1+t_l^2)}}{\pi\nu_s\sqrt{2r}} \int_{t_l}^{t_u} \frac{dt}{\sqrt{(t_u^2 - t^2)(t^2 - t_l^2)}}, \tag{A6}$$

where $t_u = \tan\frac{\phi_u}{2}$ and $t_l = \tan\frac{\phi_l}{2}$, $t = \tan\frac{\phi}{2}$, and $d\phi = \frac{2dt}{1+t^2}$. Thus the synchrotron tune is given by

$$\frac{Q_s}{\nu_s} = \frac{\sqrt{2r}\pi t_u}{\sqrt{(1+t_u^2)(1+t_l^2)}} \frac{1}{K(k_2)}, \tag{A7}$$

where modulus $k_2 = \frac{\sqrt{t_u^2 - t_l^2}}{t_u}$.

## APPENDIX B: ACTION-ANGLE VARIABLES

Using the generating function

$$F_2(\phi, J) = \int_{\hat{\phi}}^{\phi} \delta(\phi')d\phi', \tag{B1}$$

the angle variable is obtained from

$$\begin{aligned}\psi &= \frac{\partial F_2}{\partial J} = \frac{\partial E}{\partial J}\int_{\hat{\phi}}^{\phi}\frac{\partial\delta}{\partial E}d\phi' = \frac{Q_s}{\nu_s}\int_{\hat{\phi}}^{\phi}\frac{d\phi}{\delta}. \\ &= \frac{Q_s}{\nu_s}\frac{(1+t_0^2)}{t_0\sqrt{1+2t_0^2}}\int_1^{\tau}\frac{d\tau}{\sqrt{(1-\tau^2)(\frac{1}{1+2t_0^2}+\tau^2)}} \\ &= \frac{Q_s}{\sqrt{2}\nu_s}\frac{\sqrt{1+t_0^2}}{t_0}u,\end{aligned} \tag{B2}$$

with

$$u = \int_1^{\mathrm{cn}u} \frac{dx}{\sqrt{(1-x^2)(k'^2+k^2x^2)}}, \quad k' = \sqrt{1-k^2},$$

where $k = \sqrt{\frac{1+2t_0^2}{2(1+t_0^2)}}$ and the Jacobian elliptical function, cn$u$, is given by

$$\mathrm{cn}u = \frac{\tan\frac{\phi}{2}}{\tan\frac{\hat{\phi}}{2}} = \frac{2\pi}{kK(k)} \sum_{n=0}^{\infty} \frac{q^{n+1/2}}{1+q^{2n+1}} \cos[(2n+1)\psi], \tag{B3}$$

with $q = e^{-\pi K'/K}$, $K' = K(\sqrt{1-k^2})$ and

$$\psi = \frac{\pi u}{2K(k)}. \tag{B4}$$

From Eq. (B3), one obtains

$$\phi = 2\arctan\left(\tan\frac{\hat{\phi}}{2}\mathrm{cn}u\right), \tag{B5}$$

and from Hamilton's equation of motion, one gets

$$\delta = -2\sqrt{2}\sin\left(\frac{\hat{\phi}}{2}\right)\tan\left(\frac{\hat{\phi}}{2}\right)\frac{\mathrm{sn}u\ \mathrm{dn}u}{1+[\tan\frac{\hat{\phi}}{2}\mathrm{cn}u]^2}. \tag{B6}$$

When the voltage ratio is not equal to 0.5, Eqs. (B4–B6) remain valid provided that the modulus is replaced by $k_1$ of Eq. (A5) or $k_2$ of Eq. (A7).

## APPENDIX C: RESONANCE STRENGTH FUNCTION

### *Appendix C1: The $g_n$ Factor*

We expand $\delta$ in a Fourier series with

$$\delta = \sum_{n=-\infty}^{\infty} g_n(J)e^{in\psi}, \tag{C1}$$

where $g_n(J)$ can be obtained from the inverse Fourier transform,

$$g_n = \frac{1}{2\pi}\int_{-\pi}^{\pi} \delta e^{-in\psi}d\psi. \tag{C2}$$

Using Eq. (B5) and the transformation $d\psi = \frac{Q_s}{\nu_s\delta}d\phi$, we obtain

$$g_n = \frac{inQ_s}{\pi\nu_s}\int_{-\pi}^{\pi} e^{-in\psi}\arctan\left[\tan\frac{\hat{\phi}}{2}\mathrm{cn}\left(\frac{2K\psi}{\pi}\right)\right]d\psi. \tag{C3}$$

The task is to evaluate the integral,

$$I = \int_{-\pi}^{\pi} e^{-in\psi} \arctan\left[\tan\frac{\hat{\phi}}{2}\mathrm{cn}\left(\frac{2K\psi}{\pi}\right)\right] d\psi. \tag{C4}$$

To evaluate this integral, we integrate the complex function

$$e^{-inz} \arctan\left[\tan\frac{\hat{\phi}}{2}\mathrm{cn}\left(\frac{2Kz}{\pi}\right)\right]$$

along the parallelogram ABCD with vertices $-\pi$, $\pi$, $\pi\tau + 2\pi$, $\pi\tau$ respectively, where $\tau = i\frac{K'}{K}$. Since $\mathrm{cn}(\frac{2Kz}{\pi})$ has a period of $2\pi$, the integrands are equal along the path AD and BC, and therefore $\int_{\mathrm{DA}} + \int_{\mathrm{BC}} = 0$. On CD, $z = x + \pi(\tau + 1)$, where $x$ decreases from $\pi$ to $-\pi$ as the integrating path goes from C to D, the integral becomes

$$\begin{aligned}&\int_{\pi}^{-\pi} e^{-in(x+\pi\tau+\pi)} \arctan\left[\tan\frac{\hat{\phi}}{2}\mathrm{cn}\left(\frac{2Kx}{\pi} + 2iK' + 2K\right)\right] dx \\ &= -(-1)^n q^{-n} I,\end{aligned} \tag{C5}$$

where $q = e^{-\pi\frac{K'}{K}}$. Therefore, we have

$$\oint e^{-inz} \arctan\left[\tan\frac{\hat{\phi}}{2}\mathrm{cn}\left(\frac{2Kz}{\pi}\right)\right] dz = [1 - (-1)^n q^{-n}]I. \tag{C6}$$

On the other hand, the contour integral can be expressed as

$$\begin{aligned}&\oint e^{-inz} \arctan\left[\tan\frac{\hat{\phi}}{2}\mathrm{cn}\left(\frac{2Kz}{\pi}\right)\right] dz \\ &= -\frac{K\tan\frac{\hat{\phi}}{2}}{n\pi} \oint \frac{\mathrm{sn}\left(\frac{2Kz}{\pi}\right)\mathrm{dn}\left(\frac{2Kz}{\pi}\right)}{1 + \left[\tan\frac{\hat{\phi}}{2}\mathrm{cn}\left(\frac{2Kz}{\pi}\right)\right]^2} e^{-inz} dz.\end{aligned} \tag{C7}$$

Using the Cauchy theorem, we can evaluate the integral by finding the residue of poles of the integrand. Note first that the pole of $\mathrm{cn}(u)$, $\mathrm{sn}(u)$ and $\mathrm{dn}(u)$ are all located at $u = iK'$ and $iK' + 2K$, which lies on the integration path. However, these poles cancel each other in the integrand and lead to cancellation between the paths DA and BC discussed earlier. Thus poles of the integrand are given by the conditions

$$\pm i + \tan\frac{\hat{\phi}}{2}\mathrm{cn}\left(\frac{2Kz}{\pi}\right) = 0. \tag{C8}$$

Using the fact that $\mathrm{cn}(x+2K) = -\mathrm{cn}(x), \mathrm{cn}(-x) = \mathrm{cn}(x)$, and $\mathrm{cn}(x+K+iK') = \frac{k'}{ik\mathrm{cn}x}$, one obtains poles at

$$\pm\frac{\pi}{2K}u_0 \pm \frac{\pi}{2} + \frac{\pi\tau}{2}, \tag{C9}$$

where $u_0 = F\left(\arccos\left(\frac{\sqrt{k^2-\frac{1}{2}}}{k}\right), k\right)$ is the incomplete elliptical function of the first kind[10] The residues of Eq. (C7) at poles are respectively given by $\frac{\pm i}{2\mathrm{sn}u_0\,\mathrm{dn}u_0}$. The integral of Eq. (C7) is a sum of these four residue terms with the result

$$I = \frac{4\pi}{n}\frac{q^{n/2}}{1+q^n}\sin\frac{n\pi}{2}\cos\frac{n\pi u_0}{2K}. \tag{C10}$$

Thus the factor $g_n$ is given by

$$g_{2l+1} = i\frac{4Q_s}{\nu_s}\frac{q^{l+1/2}}{1+q^{2l+1}}\cos(2l+1)\frac{\pi u_0}{2K}\sin\frac{(2l+1)\pi}{2}. \tag{C11}$$

*Appendix C2: The $G_n$ Factor*

Similarly, we expand $\delta^2$ in a Fourier series with

$$\delta^2 = \sum_{n=-\infty}^{\infty} G_n(J)e^{in\psi}. \tag{C12}$$

Here $G_n(J)$ can be obtained from

$$G_n = \frac{1}{2\pi}\int_{-\pi}^{\pi}\delta^2 e^{-in\psi}d\psi = \frac{1}{2\pi}\frac{Q_s^2}{\nu_s^2}\int_{-\pi}^{\pi}\left(\frac{d\phi}{d\psi}\right)^2 e^{-in\psi}d\psi. \tag{C13}$$

Using the same method as discussed above, we integrate the complex function along the same contour ABCD, and obtain

$$G_n = \frac{1}{1-(-1)^n q^{\dagger n}}\oint f(z)dz, \tag{C14}$$

where

$$f(z) = \frac{8Q_s^2K^2}{\pi^3\nu_s^2}\tan^2\frac{\hat{\phi}}{2}\frac{\mathrm{sn}^2\left(\frac{2Kz}{\pi}\right)\mathrm{dn}^2\left(\frac{2Kz}{\pi}\right)}{\left[1+\tan^2\frac{\hat{\phi}}{2}\mathrm{cn}^2\left(\frac{2Kz}{\pi}\right)\right]^2}e^{-inz}. \tag{C15}$$

The second order poles of the function $f(z)$ are also given by (C9). The integration is then obtained from the sum of these four residue terms, i.e.,

$$\oint_{ABCD} f(z)dz = 2\pi i\sum_{i=1}^{4}\frac{d}{dz}[(z-z_i)f(z)]\Big|_{z=z_i}. \tag{C16}$$

Thus the $G_n$ factor becomes

$$G_n = \frac{4KQ_s^2}{\pi\nu_s^2}\frac{q^{n/2}}{1-q^n}\left[\sqrt{2}\frac{\sin\left(\frac{n\pi u_0}{2K}\right)}{\sin\left(\frac{\hat{\phi}}{2}\right)} + \frac{n\pi}{K}\cos\left(\frac{n\pi u_0}{2K}\right)\right]\cos\frac{n\pi}{2}, \tag{C17}$$

where only even harmonic exists.